Estimating optical absorption, scattering, and Grueneisen distributions with multiple-illumination photoacoustic tomography

Peng Shao,[1] Ben Cox,[2] and Roger J. Zemp[1,*]

[1]Department of Electrical and Computer Engineering, University of Alberta, 9107-116 Street, Edmonton, Alberta, Canada, T6G 2V4

[2]Department of Medical Physics and Bioengineering, University College London, Gower Street, London, WC1E 6BT, UK

*Corresponding author: zemp@ece.ualberta.ca

Received 7 December 2010; accepted 21 April 2011;
posted 10 May 2011 (Doc. ID 139156); published 22 June 2011

While photoacoustic methods offer significant promise for high-resolution optical contrast imaging, quantification has thus far proved challenging. In this paper, a noniterative reconstruction technique for producing quantitative photoacoustic images of both absorption and scattering perturbations is introduced for the case when the optical properties of the turbid background are known and multiple optical illumination locations are used. Through theoretical developments and computational examples, it is demonstrated that multiple-illumination photoacoustic tomography (MI-PAT) can alleviate ill-posedness due to absorption-scattering nonuniqueness and produce quantitative high-resolution reconstructions of optical absorption, scattering, and Gruneisen parameter distributions. While numerical challenges still exist, we show that the linearized MI-PAT framework that we propose has orders of magnitude improved condition number compared with CW diffuse optical tomography.

OCIS codes: 110.0113, 110.2990, 110.3010, 110.5120, 170.0170.

1. Introduction

Photoacoustic tomography (PAT) is a unique new imaging technology capable of generating images with high optical contrast, fine ultrasonic spatial resolution, and good imaging depth [1]. Despite its recent attention in the bioimaging community, presently, quantitative reconstruction of optical properties in photoacoustic imaging is rather challenging for several reasons. First, photoacoustic signals emitted from a subcutaneous location are proportional to the unknown optical fluence, which is, in turn, a function of the distributed optical properties to be estimated. This introduces a nonlinear relationship between the measured signals and the optical properties to be recovered. Second, a given optically induced heating distribution could be produced by multiple possible optical property distributions. Furthermore, the Grueneisen parameters may vary between tissue types. The present project proposes an inversion methodology that addresses each of these challenges.

A number of methods have emerged for quantitative estimation of optical properties using photoacoustics. Cox *et al.* [2] proposed a fixed-point

0003-6935/11/193145-10$15.00/0

iterative inversion scheme to recover absorption coefficient distribution when the scattering distribution is known. Yuan and Jiang [3] reconstructed an absorption coefficient map based on the finite-element solution to the diffuse equation. Ripoll and Ntziachristos [4] also described an iterative diffusion-regime inverse method that can recover small perturbations in the absorption coefficient distribution when the optical properties of the background turbid medium are known. Jetzfellner *et al.* [5] investigated the experimental performance of an iterative approach and found that it was sensitive to errors in the scattering coefficient. Banerjee *et al.* [6] proposed a noniterative scheme to recover the absorption coefficient map, which is applicable to only highly scattering media. Yin *et al.* [7] suggested iteratively estimating absorbed energy density with PAT and the interior fluence distribution with diffusing light measurements, and then calculating the absorption coefficient with quotient of the two quantities. Yuan *et al.* [8] proposed the use of a method based on the diffusion equation with *a priori* structural information from PAT images serving as a means of regularization. Unfortunately, the PAT image may be biased by the nonuniform fluence and thus the *a priori* structural information from the PAT image may not be reliable. Cox *et al.* [9] further extended the work of previous literature to the case where both absorption and reduced scattering coefficients were unknown. He showed that multiple optical wavelengths, with prior information about the wavelength dependence of the optical scattering, could overcome nonuniqueness and estimate chromophore distributions quantitatively, albeit with some numerical challenges. Guo *et al.* [10] proposed a self-calibrating method to quantify absorption coefficient. By taking the ratio of acoustic spectrals of two optical wavelengths, factors such as system bandwidth and acoustic attenuation are canceled out. This method is robust to absolute fluence variations. However, it requires the fluence to follow the Beer–Lambert law and so it is not generally applicable to heterogeneous media. With the exception of the diffuse optical tomography (DOT)-PAT hybrid technologies [7], the literature cited thus far has considered only a single optical illumination location.

One of the common elements lacking in the aforementioned literature is the inability to decouple the Greuneisen parameter from the reconstructed optical parameter distributions. The Grueneisen parameter Γ is a unitless thermodynamical parameter quantifying the efficiency of conversion between thermal energy and acoustic energy. It is given as $\Gamma = \beta c^2/C_p$, where β is the volume thermal expansivity of the tissue, c is the speed of sound in the tissue, and C_p is the specific heat capacity at a constant pressure. While most reconstruction strategies assume that the Grueneisen parameter is considered spatially constant, Cox *et al.* [11] point out that the Grueneisen parameter may vary considerably between tissue types such as fat and blood.

Additionally, the Grueneisen parameter is highly temperature dependent, and several groups have shown how photoacoustics can track temperature changes by tracking variations in photoacoustic amplitude with temperature [12–19]. In applications such as thermal therapy, where imaging of local heating is desired, the Grueneisen coefficient may vary spatially and may change as much as a few percent per degree Celcius temperature rise [13]. To our knowledge, recent articles investigating photoacoustic thermometry tracked only changes in the photoacoustic signals due to temperature sensitivity of the Grueneisen parameter and did not consider the reconstruction of this parameter. As with other temperature imaging methods [20–24], those methods requiring pre- and postheating of images are susceptible to motion artifacts and other physiological changes that often confound reliable temperature estimates. Imaging of the Grueneisen parameter may lead to opportunities for quantifying temperature distributions without confounding issues of tissue motion, although this remains to be seen.

There has been little work done in quantitative photoacoustic reconstruction of optical properties when multiple optical source locations are involved. Zemp *et al.* [25] and Ranasinghesagara *et al.* [26] described a simple method for estimating optical scattering properties of turbid media using multiple surface illumination locations. That work also described a design for flexible light delivery with accompanying photoacoustic detection. Multiple optical sources are routinely used in DOT. Multiple source–detector pair measurements are collected and then reconstructed to form images of absorption, scattering, and fluorescence with this technique. Unfortunately, DOT is limited to light collection from surface detectors. One potential advantage of multiple optical source photoacoustic imaging is that, for each optical source, photoacoustic detection effectively provides an optical fluence measurement at each subsurface location and hence subsurface points can be viewed as virtual detectors. Bal and Uhlmann [27] showed mathematically that absorption and diffusion coefficients can, in principle, be stably constructed from "internal data" corresponding to "$2n$ well-chosen boundary conditions," where n is the dimension. By "internal data," they mean PAT images, and by "boundary conditions," they mean illumination patterns. Their work, however, provided no computational or experimental studies nor a way to find the "well-chosen boundary conditions." Our work could be viewed as a first step in assessing the practicality of concepts they discuss, but from a very different theoretical perspective.

We recently proposed a novel reconstruction methodology utilizing faithful photoacoustic reconstructions of initial pressure distributions due to spatially distinct multiple illuminations (MI) [28]. We call the technique MI-PAT. We showed that absolute reconstructions of absorption coefficient perturbations is possible with simulated data, and that

these MI-PAT reconstructions are robust to spatially varying Grueneisen coefficients.

Building on that success, the goal of this paper is to show that photoacoustic imaging with multiple optical illumination locations (sources) can provide quantitative estimates of tissue optical absorption and scattering perturbations with ultrasonic spatial resolution. For a given optical illumination geometry, a heating distribution can be reconstructed via PAT. The heating distribution can, however, be due to multiple possible absorption-scattering distribution pairs, hence, nonuniqueness confounds quantitative reconstruction methods when both absorption and scattering distributions are unknown. We demonstrate that alternative illumination geometries can alleviate this type of ill-posedness and that distributions of the optical absorption and diffusion coefficients may be faithfully reconstructed, albeit with some numerical challenges. To our knowledge, this is the first report of a framework for reconstruction of both absorption and scattering coefficient distributions in a known turbid tissue with a single optical wavelength. Suggestions for further reducing ill-conditioning are discussed. One unique aspect of our framework is that our reconstruction methods are immune to and able to recover spatially varying Grueneisen parameter distributions, which may be important in practice due to large variations in this parameter for different tissue types or when temperature varies in an imaging subject. We also compare conditioning (singular values) of our methods with CW-DOT and show that MI-PAT is orders of magnitude less ill-posed.

2. Theory

We assume that the true subcutaneous heating distribution at object location $\mathbf{r}$ due to a laser pulse incident at location $\mathbf{r}_{s_i}$ is given as

$$h_i(\mathbf{r}) = \mu_a(\mathbf{r})\Phi(\mathbf{r}, \mathbf{r}_{s_i}), \tag{1}$$

where μ_a and Φ are the optical absorption coefficient and the optical fluence, respectively. Local heating induces a thermoelastic expansion with initial photoacoustic pressure generation given as

$$p_i(\mathbf{r}) = \Gamma(\mathbf{r})\mu_a(\mathbf{r})\Phi(\mathbf{r}, \mathbf{r}_{s_i}), \tag{2}$$

where $\Gamma(\mathbf{r})$ is the Grueneisen parameter as a function of object position. The initial pressure distribution can be reconstructed from received photoacoustic signals $g_i(\mathbf{r}_d, t)$ as [1]

$$\hat{p}_i(\mathbf{r}) = \mathcal{O}\{g_i(\mathbf{r}_d, t)\}, \tag{3}$$

where $\mathcal{O}$ is a reconstruction operator, ultrasound detectors are located at locations $\mathbf{r}_d$, and t is time.

The reconstructed photoacoustic image due to illumination s_i can be thought of as the true initial pressure distribution filtered by an imaging system, represented as functional operator $\mathcal{H}$, which is linear but not necessarily shift invariant:

$$\hat{p}_i(\mathbf{r}) = \mathcal{H}\{p_i(\mathbf{r})\} + n = \mathcal{H}\{\Gamma(\mathbf{r})\mu_a(\mathbf{r})\Phi_i(\mathbf{r})\} + n \tag{4}$$

where n is additive noise and we use the abbreviated notation $\Phi(\mathbf{r}, \mathbf{r}_{s_i}) = \Phi_i(\mathbf{r})$. When the reconstruction is ideal, $\mathcal{H}$ is modeled as a linear shift-invariant delta function. In general, however, $\mathcal{H}$ is linear and shift variant.

A. Problem of Absorption-Scattering Nonuniqueness

Arridge and Lionheart [29] showed that, in DOT, there is a nonuniqueness between optical absorption and scattering to the extent that it is not possible to recover a unique internal absorption distribution from dc measurements of the boundary fluence unless the scattering is known. Does the same nonuniqueness plague PAT? The situation differs in two ways: first, the data for the optical inversion in PAT consist of measurements proportional to absorbed energy, h, rather than the fluence, Φ, so the data depend more strongly on absorption than scattering; second, the data consist of internal measurements, i.e., the initial pressure is known for all interior points in contrast to DOT's measurements of Φ on the boundary. Despite these differences, a similar nonuniqueness does affect PAT, although this has yet to be proven analytically. Numerical examples calculated by minimizing an error functional are given in Fig. 1 and [9].

Figure 1 shows two pairs of absorption and scattering distributions with background absorption coefficients of $0.02\,\mathrm{cm}^{-1}$ and reduced scattering coefficients of $5\,\mathrm{cm}^{-1}$. Absorption coefficient A has a

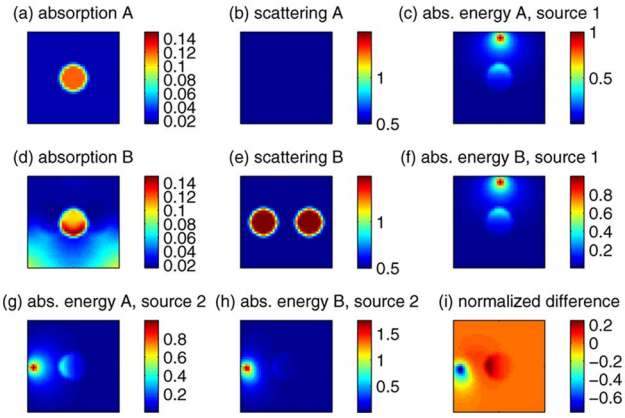

Fig. 1. (Color online) Given heating distribution (c) = (f) can be produced by the $\{\mu_a, \mu_s'\}$ distributions A $\{(a), (b)\}$ or B $\{(d), (e)\}$. Because two pairs of absorption and scattering distributions, A and B, can produce the same heating distribution for a given optical illumination geometry, approaches attempting to reconstruct optical properties using single-illumination PAT are ill-posed due to nonuniqueness. However, when illuminated by a spatially distinct alternate optical source (source 2), the heating distribution from A is distinct from that of B. The error image (difference) between (g) and (h) is shown in (i). This example demonstrates the potential to remedy nonuniqueness using multiple sources.

circular heterogeneity of $1.2\,\mathrm{cm}^{-1}$. Reduced scattering coefficient A is constant at the background value in contrast to reduced scattering coefficient B, which has the two circular scattering heterogeneities with $\mu_s' = 15\,\mathrm{cm}^{-1}$. Absorption coefficient B was calculated to ensure that the absorbed energy distributions resulting from placing a point source centrally at the top of the 20 mm × 20 mm domain were identical to machine precision. The calculations were performed using a finite-element model of light transport [30] on a 40 × 40 element square mesh with a boundary condition of zero incoming photon current.

This example shows that nonuniquenesses can appear in PAT when a single optical source is used to illuminate the sample. This makes the extraction of quantitative estimates of absorption coefficient from absorbed energy distributions difficult, if not impossible. Additional independent information is necessary in order to mitigate the nonuniqueness. As mentioned in Section 1, Cox *et al.* [9] proposed using knowledge of the wavelength dependence of the scattering in conjunction with multiple wavelengths to assist in recovering chromophore concentrations. Yin *et al.* [7] avoided the question of nonuniqueness by using DOT to estimate the fluence, thereby allowing μ_a to be estimated from $\mu_a = h/\Phi$. Here, we propose using MI patterns to provide the extra information necessary to recover absorption coefficients.

B. MI Locations as a Potential Remedy for Absorption-Scattering Nonuniqueness

The diffusive nature of light propagation in highly scattering media and the resulting randomness of the photons within the tissue at depths greater than one scattering depth might suggest that the position of the illuminating source is not a significant factor in determining a photoacoustic image at greater depths. However, when the illumination comes from just one direction, or from a small illumination region, the fluence can vary significantly within the tissue. This raises the prospect of obtaining extra information by taking PAT images of the same sample using different illumination patterns (here point sources of light are used for simplicity).

Figures 1(g) and 1(h) show the absorbed energy distributions generated from the pair of absorption and scattering coefficients calculated in Subsection 2.A but with the point source positioned centrally at the left of the image, rather than at the top. There are clearly significant differences in the images: not just around the point source itself, which is perhaps unsurprising, but also at a depth of 10 mm at the position of the absorption heterogeneity. This suggests that a set of PAT images obtained with sufficiently independently placed sources might contain sufficient additional information to enable the separation of μ_a and Φ.

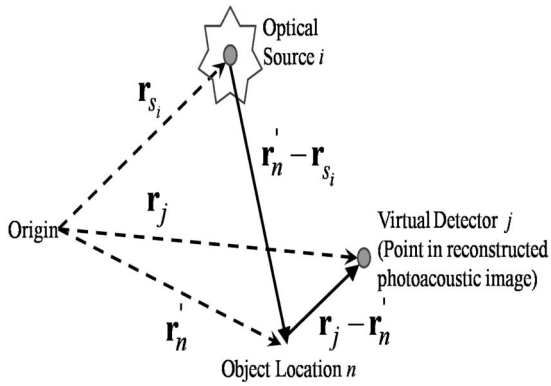

Fig. 2. Light propagation geometry.

C. Multiple Optical Source Photoacoustic Reconstruction Methododology for Absorption and Scattering Perturbations in a Known Turbid Background

Here, we consider the case where distributed absorbers perturb the fluence from the homogenous case such that

$$\Phi(\mathbf{r}_j, \mathbf{r}_{s_i}) = \Phi_0(\mathbf{r}_j, \mathbf{r}_{s_i}) + \Phi_{\mathrm{SC}}(\mathbf{r}_j, \mathbf{r}_{s_i}), \tag{5}$$

where $\Phi(\mathbf{r}_j, \mathbf{r}_{s_i})$ is the fluence at location $\mathbf{r}_j$ (with $j = 1, 2, \ldots, J$) due to illumination spot at location $\mathbf{r}_{s_i}$. Figure 2 provides an illustration of the vector geometry of the problem. $\Phi_0(\mathbf{r}_j, \mathbf{r}_{s_i})$ is the fluence due to the known homogenous turbid background with absorption and reduced scattering coefficients $\{\mu_a, \mu_s'\}$ if no additional absorption or scattering perturbations were present, and $\Phi_{\mathrm{SC}}(\mathbf{r}_j, \mathbf{r}_{s_i})$ is the fluence perturbation due to optical property variations. In this paper, we use the diffusion coefficient D, which is defined as $1/[3(\mu_a + \mu_s')]$, instead of μ_s' to depict scattering for simplicity. For both absorption and scattering perturbations such that $\mu_a(\mathbf{r}_j) = \mu_a + \delta\mu_a(\mathbf{r}_j)$ and $D(\mathbf{r}_j) = D_0 + \delta D(\mathbf{r}_j)$, we have that [31]

$$\Phi_{\mathrm{SC}}(\mathbf{r}_j, \mathbf{r}_{s_i}) = -\int \frac{\delta\mu_a(\mathbf{r}')}{D_0} G_0(\mathbf{r}_j, \mathbf{r}')\Phi(\mathbf{r}', \mathbf{r}_{s_i})\mathrm{d}\mathbf{r}' + \int \frac{\delta D(\mathbf{r}')}{D_0} \nabla G_0(\mathbf{r}_j, \mathbf{r}') \cdot \nabla\Phi(\mathbf{r}', \mathbf{r}_{s_i})\mathrm{d}\mathbf{r}', \tag{6}$$

where D_0 is the diffusion coefficient of the homogenous background, and $G_0(\mathbf{r}_j, \mathbf{r}')$ is the Green's function representing propagation from $\mathbf{r}_j \to \mathbf{r}'$. Using the first-order Born approximation, such that $\Phi_{\mathrm{SC}} \ll \Phi_0$, we have that $\Phi \approx \Phi_0$. Although this limits the inversion to the linear case, it is sufficient to show that MI ameliorates the nonuniqueness without the additional complexity the nonlinearity imposes. For cases in which the linear assumption is not sufficient, this framework can be extended to the nonlinear case, as discussed in Section 4. We can discretize the integral as

$$\Phi_{\mathrm{SC}}(\mathbf{r}_j,\mathbf{r}_{s_i})=\sum_n W^a_{\{ij\}n}\delta\mu_a(\mathbf{r}'_n)+\sum_n W^s_{\{ij\}n}\delta D(\mathbf{r}'_n) \quad (7)$$

with s_i representing a source index ($i=1,2,...,S$),

$$W^a_{\{ij\}n}=-G_0(\mathbf{r}_j,\mathbf{r}'_n)\Phi_0(\mathbf{r}'_n,\mathbf{r}_{s_i})\Delta V/D_0, \quad (8)$$

$$W^s_{\{ij\}n}=\nabla G_0(\mathbf{r}_j,\mathbf{r}'_n)\cdot\nabla\Phi_0(\mathbf{r}'_n,\mathbf{r}_{s_i})\Delta V/D_0, \quad (9)$$

where ΔV is a volume element. The $\{ij\}$ elements are grouped together in this way because they could be rastorized into a single index $k_{ij}=i+jS$ so that this may be written in matrix form as

$$\Phi_{\mathbf{SC}}=\mathbf{W}\mathbf{u}, \quad (10)$$

where $\mathbf{W}=[\mathbf{W^a}|\mathbf{W^s}]$ with $\mathbf{W^a}$ and $\mathbf{W^s}$ being $SJ\times N$ matrices corresponding to absorption and scattering, respectively. Here, $\mathbf{u}=[\delta\mu_a^T,\delta D^T]^T$, where $\delta\mu_\mathbf{a}$ and $\delta\mathbf{D}$ are $N\times 1$ column vectors. For example, $\delta\mu_\mathbf{a}=[\mu_a(\mathbf{r}'_1),\mu_a(\mathbf{r}'_2),...,\mu_a(\mathbf{r}'_N)]^T$. The locations $\{\mathbf{r}'_n: n=1,2,...,N\}$ could represent, for example, points on a mesh and represent locations at which optical properties are to be reconstructed.

If we multiply the expression for $\Phi_i(\mathbf{r}_j)\equiv\Phi(\mathbf{r}_j,\mathbf{r}_{s_i})$ by $\Gamma(\mathbf{r}_j)\mu_a(\mathbf{r}_j)$, we obtain the initial pressure distribution $p_i(\mathbf{r}_j)$ due to point source $\mathbf{r}_{s_i}$. Let us take a ratio of reconstructed initial pressure distribution estimates from photoacoustic images taken at source positions s_i and s_ℓ. If we consider locations $\{\mathbf{r}_j: j=1,2,...,J\}$, which have high signal-to-noise ratio (SNR) in the reconstructed image to avoid instability, then the ratio is well approximated as

$$\frac{\hat{p}_i(\mathbf{r}_j)}{\hat{p}_\ell(\mathbf{r}_j)}\cong\frac{\mathcal{H}\{\Phi_i(\mathbf{r}_j)\Gamma(\mathbf{r}_j)\mu_a(\mathbf{r}_j)\}}{\mathcal{H}\{\Phi_\ell(\mathbf{r}_j)\Gamma(\mathbf{r}_j)\mu_a(\mathbf{r}_j)\}}. \quad (11)$$

We now assume that the fluence distribution is slowly varying (essentially a constant) compared to the scale of a point-spread function, which should be a good approximation when absorption and scattering perturbations are not too strong. In this case, if $\mathcal{H}$ is linear and noise is small enough to be neglectable,

$$\hat{p}_i(\mathbf{r})\cong\Phi_i(\mathbf{r})\mathcal{H}\{\Gamma(\mathbf{r})\mu_a(\mathbf{r})\}. \quad (12)$$

With this approximation, the ratio becomes

$$\frac{\hat{p}_i(\mathbf{r}_j)}{\hat{p}_\ell(\mathbf{r}_j)}\cong\frac{\Phi_i(\mathbf{r}_j)}{\Phi_\ell(\mathbf{r}_j)}. \quad (13)$$

Fortuitously, the terms $\mathcal{H}\{\Gamma(\mathbf{r}_j)\mu_a(\mathbf{r}_j)\}$ cancel and we are left with a ratio of fluences due to different illumination locations. By expanding these fluence distributions in terms of homogeneous and perturbation terms, we have

$$\frac{\hat{p}_i(\mathbf{r}_j)}{\hat{p}_\ell(\mathbf{r}_j)}\cong\frac{\Phi_0(\mathbf{r}_j,\mathbf{r}_{s_i})+\Phi_{\mathrm{SC}}(\mathbf{r}_j,\mathbf{r}_{s_i})}{\Phi_0(\mathbf{r}_j,\mathbf{r}_{s_\ell})+\Phi_{\mathrm{SC}}(\mathbf{r}_j,\mathbf{r}_{s_\ell})}. \quad (14)$$

The local unknown absorption coefficients cancel and we are left with a ratio of fluences. The left-hand side represents a set of measurements, while the right-hand-side consists of model calculations. Then, Φ_{SC} is expressed in terms of the distributed absorption perturbations and we can rewrite Eq. (14) as

$$\sum_n[\hat{p}_i(\mathbf{r}_j)\mathbf{W}_{\{\ell j\}n}-\hat{p}_\ell(\mathbf{r}_j)\mathbf{W}_{\{ij\}n}]\mathbf{u}(\mathbf{r}'_n)=\hat{p}_\ell(\mathbf{r}_j)\Phi_0(\mathbf{r}_j,\mathbf{r}_{s_i})-\hat{p}_i(\mathbf{r}_j)\Phi_0(\mathbf{r}_j,\mathbf{r}_{s_\ell}). \quad (15)$$

For S optical source locations $\{s_1,s_2,...,s_S\}$, we consider $S(S-1)/2$ unique pairs $\{(s_i,s_\ell),i\neq\ell\}$ of optical sources. In matrix form, Eq. (15) is written as

$$\mathbf{Q}\mathbf{u}=\mathbf{b}, \quad (16)$$

where $\mathbf{Q}=[\mathbf{Q^a}|\mathbf{Q^s}]$ is a $[S(S-1)/2]J\times 2N$ matrix, where $\mathbf{Q^a}$ has elements $[\mathbf{Q^a}]_{\{i\ell j\}n}=\hat{p}_i(\mathbf{r}_j)\mathbf{W^a}_{\{\ell j\}n}-\hat{p}_\ell(\mathbf{r}_j)\mathbf{W^a}_{\{ij\}n}$, and $\mathbf{Q^s}$ has elements $[\mathbf{Q^s}]_{\{i\ell j\}n}=\hat{p}_i(\mathbf{r}_j)\mathbf{W^s}_{\{\ell j\}n}-\hat{p}_\ell(\mathbf{r}_j)\mathbf{W^s}_{\{ij\}n}$. These consist of measurements $\hat{p}$ from the reconstructed photoacoustic image (due to different optical source positions) and model calculations based on a known homogenous background. $\mathbf{b}$ is a $[S(S-1)/2]J\times 1$ column vector with elements $[\mathbf{b}]_{\{i\ell j\}}=\hat{p}_\ell(\mathbf{r}_j)\Phi_0(\mathbf{r}_j,\mathbf{r}_{s_i})-\hat{p}_i(\mathbf{r}_j)\Phi_0(\mathbf{r}_j,\mathbf{r}_{s_\ell})$, which are a mixture of measurements and model calculations. The unknown perturbations can be estimated quantitatively by inverting the linearized model via a Moore–Penrose pseudoinverse: $\mathbf{u}=(\mathbf{Q^TQ})^{-1}\mathbf{Q^Tb}$. We may alternatively need to use singular value decomposition to decompose the matrix $\mathbf{Q}$ as $\mathbf{Q}=\mathbf{U\Sigma V^T}$, where $\mathbf{\Sigma}$ is a diagonal matrix of singular values of the same dimension as $\mathbf{Q}$, and $\mathbf{U}$ and $\mathbf{V}$ are unitary matrices consisting of columns of the "right" and "left" singular vectors $\mathbf{u}_i$ and $\mathbf{v}_i$, respectively. The inversion is then given as $\mathbf{u}=\mathbf{V\Sigma^{-1}U^Tb}=\sum_i\frac{\mathbf{u}_i^T\mathbf{b}}{\sigma_i}\mathbf{v}_i$. Tikhanov regularization or other regularization procedures may be used to avoid instabilities due to poor matrix conditioning. It should be noted that the above should produce absolute estimates of $\{\delta\mu_a(\mathbf{r}),\delta D(\mathbf{r})\}$.

D. Recovery of the Spatially Varying Grueneisen Parameter

With the ability to recover absorption coefficients perturbations quantitatively in a way that is robust to spatially varying Grueneisen parameters, we can estimate the Grueneisen coefficient distributions as $\hat{\Gamma}(\mathbf{r})=\frac{\hat{p}(\mathbf{r})}{\hat{\Phi}(\mathbf{r})\widehat{\mu_a}(\mathbf{r})}$, where $\hat{p}(\mathbf{r})$ is the reconstructed photoacoustic image, $\widehat{\mu_a}(\mathbf{r})$ is the reconstructed absolute absorption coefficient distribution, and $\hat{\Phi}(\mathbf{r})$ is the estimated fluence distribution (computed with knowledge of the absorption perturbations). To improve robustness to noise, we choose to use all illumination sources as follows:

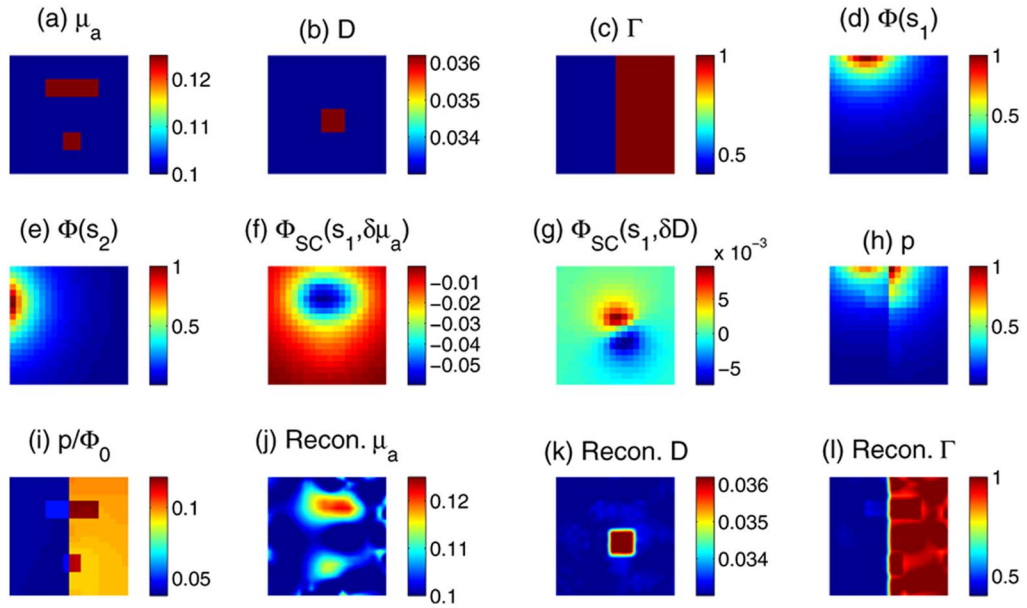

Fig. 3. (Color online) (a) True 2D μ_a distribution. (b) True 2D diffusion coefficient distribution. (c) True 2D Grueneisen parameter distribution. (d) Normalized fluence distribution from source s_1. (e) Normalized fluence distribution from source s_2. (f) Fluence perturbation from source s_1 due to only absorption perturbation. (g) Fluence perturbation from source s_1 with the presence of only diffusion coefficient perturbation. (h) Photoacoustic image with source s_1. (i) Photoacoustic image normalized by the fluence distribution Φ_0 due to source s_1, where Φ_0 is calculated under the assumption of a homogeneous medium. If the Gruneisen parameter were constant, this would represent one approximation to the absorption map. This estimate exhibits unacceptable errors. (j) Reconstructed image of the optical absorption map using our multiple-source photoacoustic inversion technique. (k) Reconstructed image of the diffusion coefficient. (l) Reconstructed image of the Grueneisen parameter.

$$\hat{\Gamma}(\mathbf{r}) = \frac{\sum_i \widehat{p_i}(\mathbf{r})}{\widehat{\mu_a}(\mathbf{r}) \sum_i \widehat{\Phi_i}(\mathbf{r})}, \tag{17}$$

where $\widehat{p_i}$ is the reconstructed photoacoustic image due to source i, and $\widehat{\Phi_i}$ is the estimated fluence distribution due to point source i.

3. Computational Reconstruction

Two-dimensional simulations are considered here for simplicity. True absorption and diffusion coefficient maps are simulated on a 20×20 grid spanning $2\,\text{cm} \times 2\,\text{cm}$, as shown in Figs. 3(a) and 3(b), respectively. The grid sampling interval is 1 mm. The reduced scattering coefficient of the turbid background is taken as $10\,\text{cm}^{-1}$ everywhere. The background absorption coefficient is taken as $\mu_a = 0.1\,\text{cm}^{-1}$, while two absorbing regions are taken to have a $0.025\,\text{cm}^{-1}$ absorption perturbation. One region of increased diffusion coefficient (reduced scattering coefficient) corresponds to a $\delta\mu_s' = 0.9\,\text{cm}^{-1}$. Eight optical sources $\{s_1, s_2, \cdots, s_8\}$, as is illustrated in Fig. 4, located 3 mm back from each edge around the object are simulated. The fluence due to source s_1 is shown in Fig. 3(d). The 3 mm gap between the tissue surface and the reconstruction region permits isotropic point sources in an infinite medium to be used as a good approximation to the true pencil-beam illumination situation that would occur in an experiment. Photoacoustic images are simulated by multiplying the computed optical fluence distribution, Grueneisen parameter distribution and the absorption map, as shown in Fig. 3(h). One way to estimate the absorption perturbations could be to estimate the local fluence as $\Phi_0(\mathbf{r})$, the fluence computed in a homogenous medium with no absorption perturbations. By normalizing the photoacoustic images by

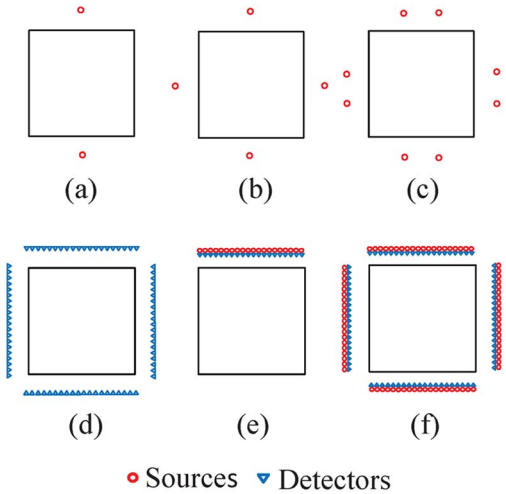

Fig. 4. (Color online) Simulation configurations. (a)–(c) two, four, and eight sources located around the object for MI-PAT and DOT imaging simulation. (d) Detector distribution for DOT imaging when using two, four, and eight sources. (e) 20 source–detector pairs positioned on top of the object for DOT. (f) 80 source–detector pairs around the tissue. For all configurations, sources and transducers are positioned 3 mm back from the object surfaces.

these fluence estimates, we produce estimates of the absorption map, as shown in Fig. 3(i) for source s_1 as an example. These estimates possess unacceptable errors that we aim to correct with the reconstruction method described in this article. When we apply our algorithm to the "measured" photoacoustic images, we are able to produce a fairly good estimate of the optical absorption map, as shown in Fig. 3(j). Reconstructed diffusion (scattering) distribution map is shown in (k). No crosstalk has been found in the two recovered maps. The maximum error without additive noise is less than 12 orders of magnitude below the true values. However, we find the reconstruction quality deteriorates quickly as the amount of noise increases, revealing sensitivity of the algorithm to noise. In the examples we show here, SNR of the simulation photoacoustic images at each detection location is no lower than 40 dB, and only data with SNR higher than 60 dB for each source pair are used for reconstruction to ensure the image quality. Key to numerical stability and robustness to noise is the conditioning of the matrix $\mathbf{Q}$. We plot the singular values of $\mathbf{Q}$ (normalized by the maximal value of each curve to compare the condition numbers) in Fig. 5. We find that the matrix condition number improves with the number of optical sources used for condition numbers of corresponding cases). With two optical sources, Eq. (16) is underdetermined. For two sources, $\mathbf{Q}$ is of size $J \times 2N$ with $J = N = 20^2$, hence there are only 400 rather than 800 singular values. Matrix conditioning improves by using four sources rather than two, and further improves by using eight. Interestingly, the diffusion coefficient seems to be reconstructed with higher accuracy than the absorption coefficient despite the fact that photoacoustic signals, in reality, are more sensitive to absorption. This is consistent with the fact that the matrix condition number of $\mathbf{Q}^a$ is larger than that of $\mathbf{Q}^s$ for the case of eight sources (data not shown). The nature of our inversion strategy might account for this phenomenon. Based on our assumptions, the ratio of photoacoustic signals is simplified into a ratio of fluences, which is sensitive to scattering perturbations. We also plot singular values from the linearized CW-DOT technique [31] when recovering optical properties. Three kinds of configuration were used for the CW-DOT imaging, as is shown in Fig. 4. In the first one, the same sources locations as the MI-PAT simulation are used, but only diffuse reflectance of light exiting from four tissue surfaces were measured by detectors for the imaging task. A more realistic configuration is to place all 20 sources and 20 detectors on top of the turbid tissue (also with a 3 mm gap from the tissue edge). Finally, we also consider 80 sources and 80 detectors placed around the object as a case where the DOT simulations are not underdetermined (but are still ill-conditioned).

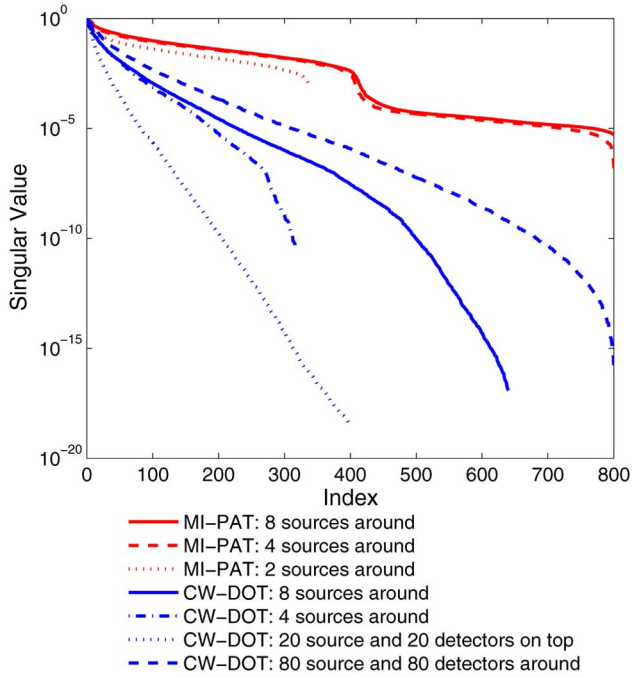

Fig. 5. (Color online) Singular value spectra (normalized by the largest value) of the matrix $\mathbf{Q}$ used in the example of Fig. 3 for recovering both absorption and scattering perturbations. For $n = 2$ sources, the number of singular values is underdetermined. Matrix conditioning improves when using more sources. The MI-PAT method is better conditioned than DOT imaging.

The condition number of a matrix, defined as the ratio of maximum to minimum singular values, typically determines the numerical stability of inversion. Compared with CW-DOT, while trying to accomplish the same imaging task with the same number of sources, the MI-PAT scheme has a condition number that is orders of magnitude smaller, which implies that it is better conditioned and thus more informative (refer to Table 1 for the overdetermined cases). The positioning of the sources matters, too. We found that sources positioned around the object were more informative than cases with sources all on the top of the object. It is interesting to note that our simulations could recover the $\{\mu_a, \mu_s'\}$ distributions accurately with only three sources (data not shown), albeit with a matrix condition number that is orders of magnitude worse, hence more sensitivity to noise. Nevertheless, this point is interesting because the work of Bal and Uhlmann [27] predict $2n = 4$ sources are needed for stable reconstruction (where $n = 2$ is the dimension of the space in our simulations). They also point out (mathematically) that fewer than $2n$ illumination patterns are possible at the expense of reconstruction stability. Our findings support their theory.

Table 1. Condition Number for Different Configurations

Case	Condition Number
MI-PAT, eight sources around	1.9654*e*5
MI-PAT, four sources around	7.3810*e*6
CW-DOT, 80 sources and 80 detectors around	1.0776*e*16

4. Discussion

We have demonstrated an inversion method to recover both absorption and scattering perturbations in a known homogeneous turbid background when multiple optical source locations are used. A number of approaches have been discussed in the literature to recover absorption-only perturbations without multiple sources. Recovery of both absorption and scattering perturbations, however, has remained a challenge. In part this is due to the ill-posedness associated with absorption-scattering nonuniqueness. We have demonstrated that the nonuniqueness problem is remedied by the use of multiple optical source illumination locations. The method presented here is not iterative, is not underdetermined (although like many methods may be ill-conditioned), and is the first, to our knowledge, to address multiple optical sources in a quantitative photoacoustic reconstruction framework. Very little has been done to recover optical properties using photoacoustics when the Grueneisen parameter $\Gamma(\mathbf{r})$ (note $\kappa(\mathbf{r}) \propto \Gamma(\mathbf{r})$) is spatially varying. Surveying the literature, Cox *et al.* [11] noted that the Grueneisen parameter Γ can vary considerably between different tissue types and, as such, may serve as a significant challenge for quantitative photoacoustic inversion of optical properties. Because the present framework can reconstruct optical properties independently of the local Grueneisen parameter, we believe it worthwhile to explore further. From the ability to estimate tissue optical properties, we can predict local fluence and hence estimate the Grueneisen parameter distribution, which may have diagnostic value in and of itself, but may also prove important for temperature imaging due to the temperature dependence of this parameter.

While our theoretical framework accounts for a spatiotemporal system response, the present simulations are restricted to an ideal photoacoustic imaging system response. For the theoretical developments to work when a more realistic imaging system is used, the conditions for the approximations discussed must hold well (i.e., the fluence must be slowly varying compared to the size of the point-spread function, and spatial variations of optical properties must not be too strong), otherwise additional errors will be introduced and reconstructions may fail.

We believe that ill-conditioning arises due to the diffusive nature of light propagation in tissue. Matrix condition number worsens with penetration depth—or equivalently, the dynamic range of fluence values throughout the image (data not shown). Illumination from points around the object rather than just the top surface was shown to be significantly advantageous in this regard. A challenge our framework faces is its sensitivity to data noise. This may be due to our hypothesis behind the derivation of the ratiometric quantity in Eq. (16). As such, we only consider points in the photoacoustic images that have a high SNR. The SNR of photoacoustic images is important to avoid reconstruction instabilities when matrix condition numbers are large. Although we use only high SNR locations as virtual detectors, we must have enough source–(virtual) detector pair combinations to produce adequate estimates of the subsurface fluence and absorption distributions if we have an adequate number of optical sources. In the presence of increasing amounts of noise, we found that regularization methods become important. Investigation of various regularization schemes to stabilize the inversion should be a topic of future work.

When the linear assumption made in Section 2 proves restrictive, the inversion scheme could be extended to nonlinear case in a number of ways. Iterations of the present method may be attempted, and should be the subject of future work. This will entail computations of Jacobian matrices $\mathbf{J} = \left[\frac{\partial \Phi}{\partial \mu_a}, \frac{\partial \Phi}{\partial \mathbf{D}}\right]$ (e.g., using finite-element methods) at each iteration, rather than using the analytical Green's function approximation $\mathbf{J} \approx \mathbf{W}$ for a homogenous turbid background. Then, the $k + 1^{th}$ iteration of the optical properties $\mathbf{u}^{k+1}$ would use the previous iteration's estimates as follows: $\mathbf{u}^{k+1} = \mathrm{inv}(\mathbf{Q}^k)\mathbf{b}^k$, where $\mathbf{Q}^k$ and b^k are the k^{th} estimate of the $\mathbf{Q}$ matrix and $\mathbf{b}$ vector, respectively. However, for large scale three-dimensional (3D) reconstruction, the Jacobian matrix might be computationally expensive and requires large memory space. To overcome this problem, Gao *et al.* [32] proposed a gradient-based method for quantitative photoacoustic imaging. Alternatively, techniques for the inversion of a Born series for diffuse waves could be exploited [33]. More generally, nonlinear optimization-based schemes for image reconstruction should be considered, which additionally permits various constraints to be included as terms modifying an objective function. For example, Gao *et al.* [34] proposed using the Bregman method combined with the total variation regularization for recovering both absorption and scattering information in turbid media with photoacoustic imaging. Numerical simulation showed that their methods surpass Jacobian matrix-based methods in terms of computational efficacy. Furthermore, piecewise features can be better reserved with the proposed regularization scheme. Nevertheless, The present linearized inversion problem could serve as a starting point for such iterative procedures. 3D reconstructions should be tested numerically, then, future work should, of course, involve experiments to test the practicality of our methods.

Combining multiple optical source locations with multiwavelength photoacoustic imaging may provide quantitative estimates of chromophore concentrations that, in turn, may pave the way for reliable mapping of oxygen saturation of hemoglobin and quantitative molecular imaging applications. Additionally, similar to Cox *et al.* [9], prior knowledge of the wavelength dependence of the scattering coefficient may further alleviate ill-conditioning and absorption-scattering nonuniqueness. This list

of future projects can now proceed given the present groundwork.

5. Summary and Conclusions

We have presented, for the first time to our knowledge, a theoretical framework and numerical results for quantitative estimation of optical properties with multiple-source photoacoustic optical tomography. The reconstruction algorithm presented is able to reproduce optical absorption, scattering, and Grueneisen distributions in a known turbid media background with high accuracy. Compared with CW-DOT, our methods are better conditioned. We also show the reconstruction of spatially varying Grueneisen parameter for the first time. Despite some challenges our method faces in terms of robustness to noise, this article may be a first step toward a number of techniques for quantitative reconstruction of optical properties with high spatial resolution.

Appendix A: Models of Light Transport

For monochromatic light, the diffusion equation of optical transport can be written as [31]

$$\frac{\partial \Phi(\mathbf{r},t)}{\partial t} + c\mu_a \Phi(\mathbf{r},t) - c\nabla \cdot [D\nabla \Phi(\mathbf{r},t)] = q(\mathbf{r},t), \tag{A1}$$

where q denotes the photon density source strength, c is the speed of light in the medium, and D is the diffusion coefficient. For photoacoustic imaging, we often use lasers with multiple-nanosecond pulse lengths. Over a time scale of a few nanoseconds, light can propagate distances of meters, whereas we are concerned with centimeter distance scales for biological imaging applications, hence, we can effectively consider q to be time independent for our present purposes.

If we assume that all light propagation, scattering, and absorption will finish in a time scale much shorter than the acoustic time scale, the optical part of the propagation is independent of time. For a time-independent point source $q(\mathbf{r},t) = A\delta(\mathbf{r})$ of strength A in an effectively infinite turbid homogeneous medium, we have

$$\mu_{\text{eff}}^2 \Phi_0(\mathbf{r}) - \nabla^2 \Phi_0(\mathbf{r}) = \frac{A}{cD}\delta(\mathbf{r}), \tag{A2}$$

where $\mu_{\text{eff}} = \sqrt{\mu_a/D}$. Taking the spatial Fourier transform, this equation can be written as

$$[k^2 + \mu_{\text{eff}}^2]\Phi_0(\mathbf{k}) = \frac{A}{cD}, \tag{A3}$$

where k is the magnitude of $\mathbf{k}$, the spatial frequency vector conjugate to $\mathbf{r}$. The solution in 3D space is given by taking the inverse Fourier transform of $\Phi_0(\mathbf{k})$ as

$$\Phi_0(\mathbf{r}) = A\frac{\exp(-\mu_{\text{eff}} r)}{4\pi cDr}, \tag{A4}$$

where $r = |\mathbf{r}|$. For two-dimensional (2D) space, the solution is found as the inverse Hankel transform of $\Phi_0(\mathbf{k})$, which is

$$\Phi_0(\mathbf{r}) = \frac{1}{2\pi}\frac{A}{cD}K_0(\mu_{\text{eff}} r), \tag{A5}$$

where K_0 is the modified Bessel function of the second kind of order zero. The 2D solution will prove useful for proof-of-principle numerical studies. The corresponding Green's functions solution to $\mu_{\text{eff}}^2 G_0(\mathbf{r},\mathbf{r}') - \nabla^2 G_0(\mathbf{r},\mathbf{r}') = \delta(\mathbf{r})$ for 3D and 2D are

$$G_0(\mathbf{r},\mathbf{r}') = \frac{\exp(-\mu_{\text{eff}}|\mathbf{r}-\mathbf{r}'|)}{4\pi|\mathbf{r}-\mathbf{r}'|}, \tag{A6}$$

$$G_0(\mathbf{r},\mathbf{r}') = \frac{1}{2\pi}K_0(\mu_{\text{eff}}|\mathbf{r}-\mathbf{r}'|), \tag{A7}$$

respectively.

Our modeling requires computation of the gradients of both $G_0(\mathbf{r},\mathbf{r}')$ and Φ. Because of radial symmetry about the source,

$$\nabla G_0(\mathbf{r}_j,\mathbf{r}') = \hat{\mathbf{r}}\frac{\partial G_0(\mathbf{r}_j,\mathbf{r}')}{\partial r}. \tag{A8}$$

For the 2D models, the Green's function is given by Eq. (A7), and using properties of Bessel functions,

$$\frac{\partial K_0(\mu_{\text{eff}} r)}{\partial r} = -\mu_{\text{eff}} K_1(\mu_{\text{eff}} r). \tag{A9}$$

Hence, for 2D, Eq. (9) becomes

$$W^s_{\{ij\}n} = -\frac{1}{4\pi^2}\frac{A\mu_{\text{eff}}^2}{cD_0}K_1(\mu_{\text{eff}}|\mathbf{r}_j - \mathbf{r}'_n|) \times K_1(\mu_{\text{eff}}|\mathbf{r}'_n - \mathbf{r}_{s_i}|)\frac{(\mathbf{r}_j - \mathbf{r}'_n)\cdot(\mathbf{r}'_n - \mathbf{r}_{s_i})}{|\mathbf{r}_j - \mathbf{r}'_n||\mathbf{r}'_n - \mathbf{r}_{s_i}|}\frac{\Delta V}{D_0}. \tag{A10}$$

This research was sponsored by the Canadian Cancer Society (grants NCIC TFF 019237 and 019249), the Natural Sciences and Engineering Research Council of Canada (grant NSERC 355544-08), and the Engineering and Physical Sciences Research Council UK (EPSRCUK).

References

1. M. H. Xu and L. H. V. Wang, "Photoacoustic imaging in biomedicine," Rev. Sci. Instrum. **77**, 041101 (2006).
2. B. T. Cox, S. R. Arridge, K. P. Kostli, and P. C. Beard, "Two-dimensional quantitative photoacoustic image reconstruction of absorption distribution in scattering media by use of a simple iterative method," Appl. Opt. **45**, 1866–1875 (2006).
3. Z. Yuan and H. B. Jiang, "Quantitative photoacoustic tomography: recovery of optical absorption coefficient maps of heterogeneous media," Appl. Phys. Lett. **88**, 231101 (2006).

4. J. Ripoll and V. Ntziachristos, "Quantitative photoacoustic tomography: recovery of optical absorption coefficient maps of heterogeneous media," Phys. Rev. E **71**, 031912 (2005).
5. T. Jetzfellner, D. Razansky, A. Rosenthal, R. Schulz, K. H. Englmeier, and V. Ntziachristos, "Performance of iterative optoacoustic tomography with experimental data," Appl. Phys. Lett. **95**, 013703 (2009).
6. B. Banerjee, S. Bagchi, R. M. Vasu, and D. Roy, "Quantitative photoacoustic tomography from boundary pressure measurements: noniterative recovery of optical absorption coefficient from the reconstructed absorbed energy map," J. Opt. Soc. Am. A **25**, 2347–2356 (2008).
7. L. Yin, Q. Wang, Q. Z. Zhang, and H. B. Jiang, "Tomographic imaging of absolute optical absorption coefficient in turbid media using combined photoacoustic and diffusing light measurements," Opt. Lett. **32**, 2556–2558 (2007).
8. Z. Yuan, Q. Wang, and H. B. Jiang, "Reconstruction of optical absorption coefficient maps of heterogeneous media by photoacoustic tomography coupled with diffusion equation based regularized newton method," Opt. Express **15**, 18076–18081 (2007).
9. B. T. Cox, S. R. Arridge, and P. C. Beard, "Estimating chromophore distributions from multiwavelength photoacoustic images," J. Opt. Soc. Am. A **26**, 443–455 (2009).
10. Z. Guo, S. Hu, and L. V. Wang, "Calibration-free absolute quantification of optical absorption coefficients using acoustic spectra in 3D photoacoustic microscopy of biological tissue," Opt. Lett. **35**, 2067–2069 (2010).
11. B. T. Cox, J. G. Laufer, and P. C. Beard, "The challenges for quantitative photoacoustic imaging," Proc. SPIE **7177**, 717713 (2009).
12. I. V. Larina, K. V. Larin, and R. O. Esenaliev, "Real-time optoacoustic monitoring of temperature in tissues," J. Phys. D **38**, 2633–2639 (2005).
13. M. Pramanik, T. N. Erpelding, L. Jankovic, and L. V. Wang, "Tissue temperature monitoring using thermoacoustic and photoacoustic techniques," Proc. SPIE **7564**, 75641Y (2010).
14. S. Y. Emelianov, S. R. Aglyamov, A. B. Karpiouk, S. Mallidi, S. Park, S. Sethuraman, J. Shah, R. Smalling, J. M. Rubin, and W. G. Scott, "Synergy and applications of combined ultrasound, elasticity, and photoacoustic imaging," Proc. IEEE Ultrason. Symp. **2006**, 405–415 (2006).
15. J. Shah, S. R. Aglyamov, K. Sokolov, T. E. Milner, and S. Y. Emelianov, "Ultrasound-based thermal and elasticity imaging to assist photothermal cancer therapy," J. Biomed. Opt. **13**, 034024 (2008)
16. S. Sethuraman, S. R. Aglyamov, R. W. Smalling, and S. Y. Emelianov, "Remote temperature estimation in intravascular photoacoustic imaging," Ultrasound Med. Biol. **34**, 299–308 (2008).
17. J. Shah, S. Park, S. R. Aglyamov, T. Larson, T. Ma, L. Sokolov, K. Johnston, T. E. Milner, and S. Y. Emelianov, "Photoacoustic imaging and temperature measurement for photothermal cancer therapy," J. Biomed. Opt. **13**, 034024 (2008).
18. S. H. Wang, C. W. Wei, S. H. Jee, and P. C. Li, "Photoacoustic temperature measurements for monitoring of thermal therapy," Proc. SPIE **7177**, 71771S (2009).
19. M. Pramanik and L. H. V. Wang, "Thermoacoustic and photoacoustic sensing of temperature," J. Biomed. Opt. **14**, 054024 (2009).
20. R. Seip and E. S. Ebbini, "Noninvasive estimation of tissue temperature response to heating fields using diagnostic ultrasound," IEEE Trans. Biomed. Eng. **42**, 828–839 (1995).
21. R. Maass-Moreno and C. A. Damianou, "Noninvasive temperature estimation in tissue via ultrasound echo-shifts. Part 1. Analytical model," J. Acoust. Soc. Am. **100**, 2514–2521 (1996).
22. R. Seip, P. VanBaren, C. A. Cain, and E. S. Ebbini, "Noninvasive real-time multipoint temperature control for ultrasound phased array treatments," IEEE Trans. Ultrason. Ferroelectr. Freq. Control **43**, 1063–1073 (1996).
23. S. J. Graham, M. J. Bronskill, and R. M. Henkelman, "Time and temperature dependence of MR parameters during thermal coagulation of ex vivo rabbit muscle," Magn. Reson. Med. **39**, 198–203 (1998).
24. P. Steiner, R. Botnar, B. Dubno, G. G. Zimmermann, G. S. Gazelle, and J. F. Debatin, "Radio-frequency-induced thermoablation: monitoring with T1-weighted and proton-frequency-shift MR imaging in an interventional 0.5-T environment," Radiology **206**, 803–810 (1998).
25. R. J. Zemp, J. Ranasinghesagara, Y. Jiang, X. Chen, and K. Mathewson, "A photoacoustic method for optical scattering measurements in turbid media," Proc. SPIE **7177**, 71770Q (2009).
26. J. C. Ranasinghesagara, Y. Jiang, X. H. Chen, K. Mathewson, and R. J. Zemp, "Photoacoustic technique for assessing optical scattering properties of turbid media," J. Biomed. Opt. **14**, 040504 (2009).
27. G. Bal and G. Uhlmann, "Inverse diffusion theory of photoacoustics," Inv. Prob. **26**, 085010 (2010).
28. R. J. Zemp, "Quantitative photoacoustic tomography with multiple optical sources," Appl. Opt. **49**, 3566–3572 (2010).
29. S. R. Arridge and W. R. B. Lionheart, "Nonuniqueness in diffusion-based optical tomography," Opt. Lett. **23**, 882–884 (1998).
30. S. R. Arridge, M. Schweiger, M. Hiraoka, and D. T. Delpy, "A finite element approach to modelling photon transport in tissue," Med. Phys. **20**, 299–309 (1993).
31. L. V. Wang, *Biomedical Optics: Principles and Imaging* (Wiley, 2007).
32. H. Gao, H. Zhao, and Sl Osher, "Quantitative photoacoustic tomography," University of California Los Angeles (UCLA) Computational and Applied Mathematics Reports (UCLA, 2011), Vol. 11–28.
33. S. Moskow and J. C. Schotland, "Numerical studies of the inverse Born series for diffuse waves," Inv. Prob. **25**, 095007 (2009).
34. H. Gao, H. Zhao, and S. Osher, "Bregman methods in quantitative photoacoustic tomography," University of California Los Angeles (UCLA) Computational and Applied Mathematics Reports (UCLA, 2010), Vol. 10–42.